HAL open science

Microscopic picture of the erosion and sedimentation processes in dense granular flows

Pierre Soulard, Denis Dumont, Thomas Salez, Elie Raphaël, Pascal Damman

To cite this version:

Pierre Soulard, Denis Dumont, Thomas Salez, Elie Raphaël, Pascal Damman. Microscopic picture of the erosion and sedimentation processes in dense granular flows. 2019. hal-02419372v1

HAL Id: hal-02419372

https://hal.science/hal-02419372v1

Preprint submitted on 19 Dec 2019 (v1), last revised 28 May 2020 (v2)

HAL is a multi-disciplinary open access archive for the deposit and dissemination of scientific research documents, whether they are published or not. The documents may come from teaching and research institutions in France or abroad, or from public or private research centers.

L'archive ouverte pluridisciplinaire **HAL**, est destinée au dépôt et à la diffusion de documents scientifiques de niveau recherche, publiés ou non, émanant des établissements d'enseignement et de recherche français ou étrangers, des laboratoires publics ou privés.

Microscopic picture of the erosion and sedimentation processes in dense granular flows

Pierre Soulard,[1,*] Denis Dumont,[2,*] Thomas Salez,[3,4] Elie Raphaël,[1] and Pascal Damman[2,†]

[1] *UMR CNRS Gulliver 7083, ESPCI Paris, PSL Research University, 75005 Paris, France.*
[2] *Laboratoire Interfaces & Fluides Complexes, Université de Mons, 20 Place du Parc, B-7000 Mons, Belgium.*
[3] *Univ. Bordeaux, CNRS, LOMA, UMR 5798, F-33405 Talence, France.*
[4] *Global Station for Soft Matter, Global Institution for Collaborative Research and Education, Hokkaido University, Sapporo, Japan.*

(Dated: December 19, 2019)

We introduce a novel microscopic model for gravity-driven dense granular flows at small inertial numbers, involving friction, geometry, and nonlocal collisional effects. Through the detailed description of the exchange mechanisms between a fluid phase and a solid one, the model allows to build a complete phase diagram including erosion, sedimentation, and stationary-flow regimes. The predictions are confronted to original results from discrete-element-method simulations, and to experiments from the literature. The quantitative agreement allows to characterize the size and shape of the cooperative regions, and to unify various configurations, observations, and observables from the literature.

Gravity-driven flows of granular matter are involved in a wide variety of situations, ranging from industrial processes to geophysical phenomena, such as avalanches or landslides [1]. These flows are characterized by the coexistence of solid and fluid phases, whose stability is directly related to the erosion and sedimentation processes occurring at the solid-fluid interface. This problem has not yet been solved despite the development of semi-empirical mean-field approaches [2–6]. To settle this issue, we build a microscopic model involving friction, geometry, and a nonlocal cooperativity emerging from the propagation of collisions. This picture enables us to obtain a detailed description of the exchange mechanisms between the fluid and solid phases, and ultimately a complete phase diagram of erosion and sedimentation, in quantitative agreement with experiments.

Over the last two decades, different theoretical approaches have been proposed in order to describe dense granular flows. The most widely used models are based on the $\mu(I)$-rheology [3–7]. It consists in a semi-empirical description of granular matter, through an effective friction coefficient μ function of an inertial number I. In parallel, semi-empirical models have been developed to describe the dynamics of avalanches, defined as a dense granular flow atop a static granular solid. This type of systems exhibits complex behaviours due to the intrinsic transfers between the fluid and solid phases at their interface. Specifically, the erosion of the solid phase by the avalanche feeds the fluid phase, and thus the avalanche, while the sedimentation of the fluid phase tends to stop the motion. The BCRE model was proposed to account for this coupled dynamics [2, 8, 9]. Two key ingredients are at the heart of such an approach: i) the intuitive idea that the evolution of the sharp interface between the two phases is determined by its local tilt angle θ (see Fig. 1); and ii) the assumed existence of a neutral angle θ^*, such that for $\theta > \theta^*$ erosion occurs, and for $\theta < \theta^*$ sedimentation occurs. However, while such a neutral angle is an appealing phenomenological feature, it has had no microscopic justification so far, and cannot be evaluated *a priori*.

In this Letter, we propose a microscopic description of the erosion and sedimentation processes at play in a dense granular flow driven by gravity. The model involves a flowing layer of grains over a static but erodible one, at small inertial number, and includes a nonlocal contribution related to collisions. Its predictions are directly confronted to numerical results obtained from a Discrete Element Method (DEM), in the two canonical configurations: an inclined plane and a heap. Despite its simplicity, the proposed model is able to quantitatively describe the observed phase diagram, as well as the transitions between sedimentation, stationary flow, and erosion. Moreover, the model allows to rationalize an important observable in inclined-plane experiments from the literature: the stop angle of a granular flow.

Inspired by previous works [10–12], we consider the discrete nature of a granular assembly. As schematized in Fig. 1, we introduce a bidimensional description, with a moving layer of $\mathcal{R}$ grains (counted vertically), *i.e.* the fluid phase, above a static layer, *i.e.* the solid phase. The grains are identical spheres of diameter d, and mass m, with a friction coefficient μ. The roughness of the solid-fluid interface is characterized by an angle $\varphi_{\rm sol}$ with respect to the normal to the interface, quantifying the angular depth of the hole between two grains. In the following, we focus on the motion of one single grain from the fluid phase, in contact with the solid phase. This grain is subjected to the weight of the $\mathcal{R}$ grains constituting the moving layer, and, in order to move forward, it has to frictionally slide and/or roll over the underlying static layer of grains, but no jump is allowed. The instantaneous position of the moving grain is described through

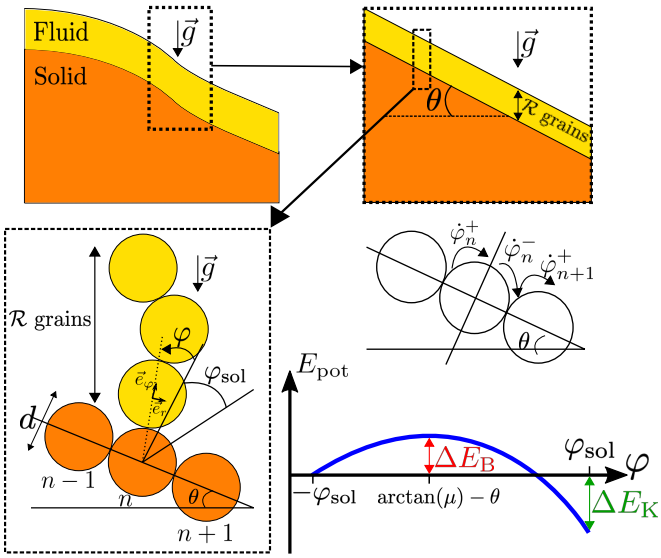

FIG. 1. A dense fluid granular phase (yellow) moves over an underlying static solid granular phase (orange). Locally, the solid-fluid interface makes an angle θ with the horizontal plane. The instantaneous position of a particular grain, moving above a static grain n, is described through the angle φ between the normal to the interface and the contact interparticle-distance unit vector $\vec{e}_r$. The moving grain starts at angular position $-\varphi_{\rm sol}$, with angular velocity $\dot{\varphi}_n^+$, and arrives at $+\varphi_{\rm sol}$, with angular velocity $\dot{\varphi}_n^-$. Also shown is the effective potential energy $E_{\rm pot}$ as a function of angular position φ, during the first step of the grain motion, within one cycle where $\varphi \in [-\varphi_{\rm sol}, +\varphi_{\rm sol}]$. The two essential features are the barrier energy $\Delta E_{\rm B}$ at maximum, and the final energy gain $\Delta E_{\rm K}$.

a single variable: the angle φ between the normal to the interface and the contact interparticle-distance unit vector $\vec{e}_r$ (see Fig. 1).

The motion is divided into two subsequent steps: first, the grain starts at angular position $-\varphi_{\rm sol}$ with angular velocity $\dot{\varphi}_n^+$, and then moves above a static grain indexed by n, until it arrives at $+\varphi_{\rm sol}$ with angular velocity $\dot{\varphi}_n^-$; secondly, it elastically collides the next static grain indexed by $n+1$, which induces a sharp change of its velocity, as well as secondary elastic collisions within the fluid and solid phases – and thus nonlocal energy transfers. A new and similar cycle then starts, with an initial angular velocity $\dot{\varphi}_{n+1}^+$. The restitution coefficient $\alpha = (\dot{\varphi}_{n+1}^+/\dot{\varphi}_n^-)^2$ is defined as the ratio between the kinetic energies of the moving grain after and before the collision.

During the first step above, the total force exerted on the moving grain is oriented along $\vec{e}_\varphi$, since the component along $\vec{e}_r$ is null in virtue of the action-reaction law. It contains two contributions: the transverse projection $\mathcal{R}mg\sin(\varphi+\theta)\vec{e}_\varphi$ of the weight and the dynamic Amontons-Coulomb friction force $-\mu\mathcal{R}mg\cos(\varphi+\theta)\vec{e}_\varphi$ generated by the normal projection of the weight on the static grain.

The total force can thus be written as $-(1/d)\mathrm{d}E_{\rm pot}/\mathrm{d}\varphi$, where $E_{\rm pot}(\varphi) = \mathcal{R}mgd\{\cos(\varphi+\theta) - \cos(\varphi_{\rm sol}-\theta) + \mu\left[\sin(\varphi+\theta)+\sin(\varphi_{\rm sol}-\theta)\right]\}$ is an effective potential for the motion (see Fig. 1), and where the origin of energies has been arbitrarily chosen at $\varphi = -\varphi_{\rm sol}$. At $\varphi = \arctan(\mu)-\theta$, this potential is maximal, resulting in an energy barrier:

$$\Delta E_{\rm B} = \mathcal{R}mgd[\sqrt{1+\mu^2} - \cos(\varphi_{\rm sol}-\theta) + \mu\sin(\varphi_{\rm sol}-\theta)] \ . \tag{1}$$

If the moving grain has enough initial kinetic energy $md^2(\dot{\varphi}_n^+)^2/2$ to overcome the barrier, it gains the kinetic energy:

$$\Delta E_{\rm K} = 2\mathcal{R}mgd\,(\sin\theta - \mu\cos\theta)\sin\varphi_{\rm sol} \ , \tag{2}$$

at the end of the first step, and its velocity becomes $\dot{\varphi}_n^- = [(\dot{\varphi}_n^+)^2 + 2\Delta E_{\rm K}/(md^2)]^{1/2}$.

Up to now, we have not considered the contacts between grains in the fluid and solid layers, leading to the nonlocal cooperative effects observed for dense granular flows. In our model, they naturally come into play during the second step of motion. Indeed, after the primary elastic collision with the $n+1^{\rm th}$ static grain (see Fig. 1), the velocity of the considered moving grain changes suddenly and secondary elastic collisions occur within the fluid and solid phases. The energy transferred by the moving grain to the static grain during the primary collision is assumed to be proportional to the incoming energy, and reads $amd^2(\dot{\varphi}_n^-)^2/2$, with a a constant prefactor comprised between 0 and 1. After the primary collision, the energies of the moving grain and the knocked static grain thus temporarily become $(1-a)md^2(\dot{\varphi}_n^-)^2/2$ and $amd^2(\dot{\varphi}_n^-)^2/2$ before the energy reallocation. Then, cascades of secondary collisions are triggered in both phases. In a minimal description, we assume that they involve: i) the numbers $\mathcal{N}_{\rm flu}$ and $\mathcal{N}_{\rm sol}$ of grains involved in the collisions in each phase; and ii) some equipartition of the energy among those grains. For the fluid phase in particular, this results in the primary energy loss of the moving grain being redistributed over the $\mathcal{N}_{\rm flu}$ moving grains – an energy reallocation that forms the essence of nonlocality. Over the primary and secondary collisions, the total energy loss ΔE_0 for the moving grain thus reads:

$$\Delta E_0 = \frac{md^2}{2}\left[(\dot{\varphi}_n^-)^2 - (\dot{\varphi}_{n+1}^+)^2\right] = \frac{amd^2}{2\mathcal{N}_{\rm flu}}(\dot{\varphi}_n^-)^2 \ . \tag{3}$$

As a consequence, the restitution coefficient must be $\alpha = 1 - a/\mathcal{N}_{\rm flu}$. Recalling the above link between $\dot{\varphi}_n^-$ and $\dot{\varphi}_n^+$ through $\Delta E_{\rm K}$, one finally gets the central recursive relation:

$$(\dot{\varphi}_{n+1}^+)^2 = \alpha\left[(\dot{\varphi}_n^+)^2 + \frac{2\Delta E_{\rm K}}{md^2}\right] \ . \tag{4}$$

Assuming a global translational invariance in the system [10–12], and thus looking for the fixed point of Eq. (4), one gets $(\dot{\varphi}_\infty^+)^2 = 2\alpha\Delta E_\mathrm{K}/[md^2(1-\alpha)]$. In this homogeneous state, during each cycle, the kinetic energy gained by the moving grain when getting down the effective potential is exactly compensated by the loss due to the subsequent collisional cascade, such that $\Delta E_\mathrm{K} = \Delta E_0$.

The homogeneous state is stable only if the associated kinetic energy $E_\mathrm{K}^\infty = md^2(\dot{\varphi}_\infty^+)^2/2 = \alpha\Delta E_\mathrm{K}/(1-\alpha)$, set by Eq. (2), is larger than the barrier ΔE_B, set by Eq. (1), giving a limiting condition :

$$\frac{\alpha}{1-\alpha}\,\Delta E_\mathrm{K}(\theta_\mathrm{sed},\mathcal{R}) = \Delta E_\mathrm{B}(\theta_\mathrm{sed},\mathcal{R})\ , \qquad (5)$$

which determines the sedimentation angle $\theta_\mathrm{sed}(\mathcal{R})$. If $\theta < \theta_\mathrm{sed}$, the lowest layer (at least) of the fluid phase stops, and $\mathcal{R}$ decreases.

A similar reasoning allows to discuss erosion. In the homogeneous state, and over one complete cycle of trajectory for the considered moving grain, the solid phase receives the energy $amd^2(\dot{\varphi}_\infty^-)^2/2 = \mathcal{N}_\mathrm{flu}\Delta E_\mathrm{K}$. Considering the total number $\mathcal{N}_\mathrm{sol}$ of static grains involved in the secondary collisions within the solid phase, and the equipartition of energy among those grains, the static grain at the solid-fluid interface receives a kinetic energy $\mathcal{N}_\mathrm{flu}\Delta E_\mathrm{K}/\mathcal{N}_\mathrm{sol}$, set by Eq. (2). The homogeneous state above is stable only if that kinetic energy remains smaller than the own energy barrier $\Delta E_\mathrm{B}(\theta,\mathcal{R}+1)$ of the static grain, set by Eq. (1). The limiting condition:

$$\frac{\mathcal{N}_\mathrm{flu}}{\mathcal{N}_\mathrm{sol}}\Delta E_\mathrm{K}(\theta_\mathrm{ero},\mathcal{R}) = \Delta E_\mathrm{B}(\theta_\mathrm{ero},\mathcal{R}+1)\ , \qquad (6)$$

determines the erosion angle $\theta_\mathrm{ero}(\mathcal{R})$. If $\theta > \theta_\mathrm{ero}$, the highest layer (at least) of the solid phase starts to flow, and $\mathcal{R}$ increases.

In order to close the set of Eqs. (5) and (6), one needs to specify further the cooperativities $\mathcal{N}_\mathrm{flu}$ and $\mathcal{N}_\mathrm{sol}$. In the bulk, for both phases, the cooperative regions contain ξ grains, and are determined by their fractal dimension D, and thus their length $\sim \xi^{1/D}$. However, if the phase thickness is smaller than $\xi^{1/D}$, the cooperative regions feel the boundaries and the bulk result might be modified. For the solid phase supported on a rigid substrate, one expects a simple reflecting boundary condition, ensuring that $\mathcal{N}_\mathrm{sol} = \xi$ is maintained. In contrast, for the fluid phase, the fluid-air interface acts as a free-volume reservoir and, as such, is expected to truncate the neighbouring cooperative regions. The number of grains in the latter becomes $\sim \xi^{1-1/D}\mathcal{R}$. This suggests a crossover from a linear behaviour in $\mathcal{R}$ to a saturation at ξ, as the ratio $\mathcal{R}/\xi^{1/D}$ overcomes 1. Therefore, we propose the Ansatz: $\mathcal{N}_\mathrm{flu}(\mathcal{R}) = \xi\left[1-\exp\left(-\mathcal{R}/\xi^{1/D}\right)\right]$.

To test the predictions of the model, we performed DEM simulations for two canonical experimental configurations. For the inclined-plane configuration (Fig. 2, top), the solid phase is made of a single layer of grains glued on the incline. The stop angle θ_stop is defined as the minimal angle of the substrate for which a flow is observed. As shown in Fig. 3, it is a decreasing function of the layer thickness $\mathcal{R}$, like in previous results [13–17]. Specifically, θ_stop first rapidly decreases before saturating to a constant value. Moreover, the DEM data are in close agreement with the experimental data reported by Pouliquen for glass beads [13]. For the heap configuration (Fig. 2, bottom), DEM simulations confirm that the heap angle θ_heap and the thickness $\mathcal{R}$ of the fluid layer self-adjust until a stationary state is reached. As shown in Fig. 3 for the latter state, θ_heap is significantly larger than θ_stop, but follows a similar monotonically decaying trend with $\mathcal{R}$ towards a saturation value.

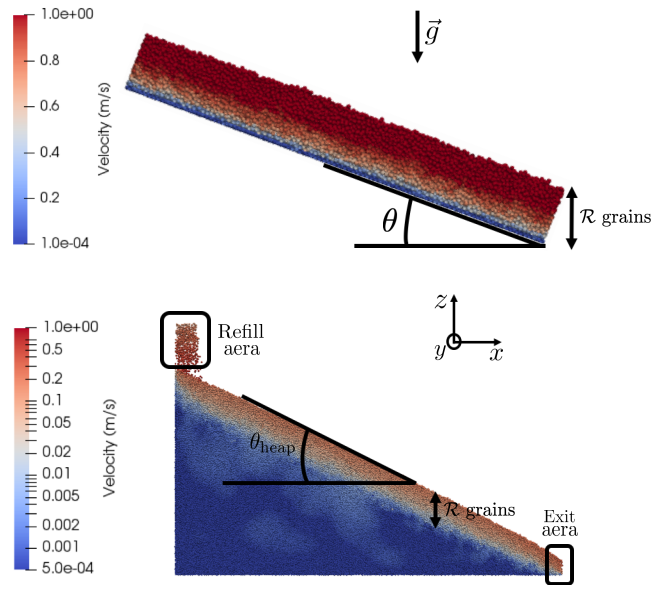

FIG. 2. Snapshots of the DEM simulations for the two canonical configurations for granular flows: (top) inclined-plane flow with fixed angle and thickness; (bottom) heap flow with fixed flow rate. The color maps refer to the velocity of each grain, as indicated in the scale bar.

We now turn to a comparison of all these observations to the predictions of our microscopic model. The evolutions of θ_sed and θ_ero with $\mathcal{R}$ can be computed numerically from Eqs. (5) and (6), provided that the five relevant dimensionless parameters of the model, μ, φ_sol, a, ξ, and D are fixed. The coefficient a was estimated to be close to 0.5 [10], while the effective friction coefficient is fixed to $\mu = \tan(20°)$ [13], and φ_sol spans the range $[23.4°, 30°]$ [18]. Thus, ξ and D are the only free parameters. As shown in Fig. 3, the model quantitatively captures all the DEM and experimental data, using the best-fit values: $\xi = 6$ and $D = 1.3$. Interestingly, these outputs suggest chain-like cooperative regions containing a few grains, which is reminiscent of the force-chain

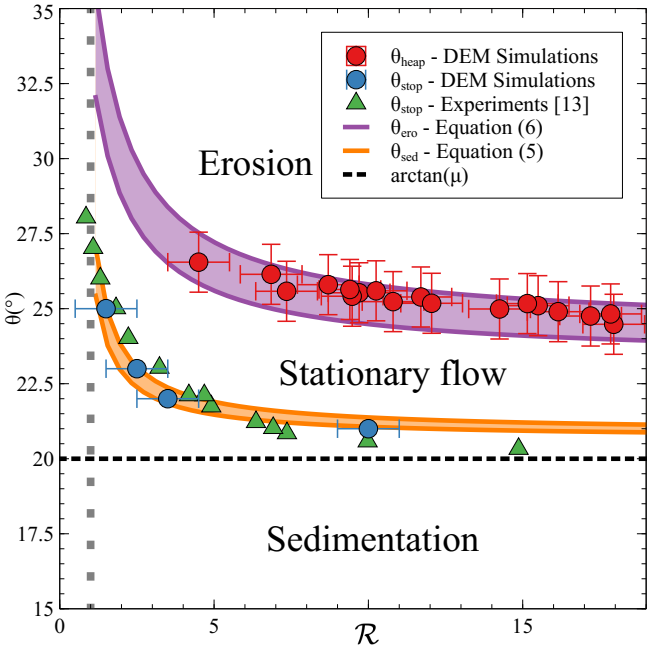

FIG. 3. The θ-$\mathcal{R}$ phase diagram. Ensemble of results from: i) DEM simulations in the two canonical configurations for granular flows, *i.e.* inclined plane ($\theta_{\rm stop}$) and heap ($\theta_{\rm heap}$) ; ii) inclined-plane experimental results ($\theta_{\rm stop}$) by Pouliquen [13] ; and iii) predictions ($\theta_{\rm ero}$, $\theta_{\rm sed}$) from the model through Eqs. (5) and (6). In the model, the fixed parameters are $\mu = \tan(20°)$ [13], $a = 0.5$ [10], and $\varphi_{\rm sol} \in [23.4°, 30°]$ (see light purple and light orange regions in the diagram) [18], and the two adjustable parameters are $\xi = 6$ and $D = 1.3$. The horizontal dashed line indicates $\theta = \arctan(\mu)$, and the vertical one indicates $\mathcal{R} = 1$.

architecture in static granular contact [19, 20].

All together, Fig. 3 embodies the θ-$\mathcal{R}$ phase diagram of granular flows, for a particular set of parameters μ, $\varphi_{\rm sol}$, a, ξ, and D. This central outcome exhibits the erosion, stationary-flow, and sedimentation domains, through their respective boundaries. Several observations can be made. First, $\theta_{\rm ero}(\mathcal{R}) > \theta_{\rm sed}(\mathcal{R})$. Therefore, stationary flows appear to exist for a continuum of angles θ comprised in between these two distinct boundaries. Interestingly, this opens a gap within the BCRE picture [8], in which a single neutral angle θ^* accounts for both the sedimentation and erosion processes. Secondly, $\theta_{\rm ero}$ and $\theta_{\rm sed}$ both decay monotonically with $\mathcal{R}$, and tend to a constant value at large $\mathcal{R}$. For $\theta_{\rm sed}$, these are direct consequences of both the energy equipartition and cooperativity truncation mechanisms. Indeed, a decrease of $\mathcal{R}$ implies that less grains share the energy loss of the considered moving grain, which renders flow and erosion more difficult. Surface flow in yielded athermal granular media thus appears to be inhibited by the truncation of the cooperativity – as opposed to surface flow in ideal supercooled liquids at equilibrium [21]. Thirdly, the saturation values are self-consistently above the ultimate solid-friction limit $\arctan(\mu)$ [13, 22]. Finally, the decay of $\theta_{\rm sed}(\mathcal{R})$ allows to justify why $\theta_{\rm stop}$ is indeed a proper measurement of $\theta_{\rm sed}$. In the inclined-plane configuration, as one decreases the angle θ, it eventually reaches $\theta_{\rm sed}(\mathcal{R})$. By definition of the latter, the lowest layer (at least) of the fluid phase stops and $\mathcal{R}$ reduces by one (or more) units. Due to its monotony, $\theta_{\rm sed}$ then increases, and the sedimentation front propagates upwards until the whole system is stopped.

This work benefited from financial support by the Fonds National de la Recherche Scientifique (FNRS, PDR research project T.0109.16 “Capture biomimétique de fluide” and CDR project J.0191.17 “Mimicking elasticity with viscous fluids”), and by the Action de Recherche Concertée (UMONS, research project “Mecafood”). D. D. acknowledges funding from FNRS (Foundation for Training in Industrial and Agricultural Research). The authors also thank Paul Rambach and Yacine Amarouchene for interesting discussions.

Methods

Model. The grains are identical spheres of diameter d, and mass m, with a friction coefficient μ between them. The latter encompasses sliding and rolling frictions, as well as geometry. The angle $\varphi_{\rm sol}$ quantifying the angular depth of the hole between two grains ranges satisfies $23.4° \leq \varphi_{\rm sol} \leq 30°$ for spherical grains in 3D [18], depending if one considers the neck between two grains or the tops.

DEM Simulations. Discrete Element Method (DEM) numerical simulations were performed by means of the software LIGGGHTS [23]. The granular media simulated were made up of monodisperse spherical beads with $d = 1$ mm. The Hertz-Mindlin model has been used to characterize the contacts between grains. The following micro-mechanical parameters were chosen: inelastic coefficient $e = 0.5$, microscopic sliding friction coefficient $\mu_{\rm s} = 0.5$, microscopic rolling friction coefficient $\mu_{\rm s} = 0.01$, Young's modulus $Y = 1$ MPa, and Poisson ratio $\nu = 0.45$.

For the inclined-plane configuration (Fig. 2, top), an horizontal periodic channel of $100d$ long and $20d$ large is filled with a chosen thickness layer of beads. The plane is inclined at an angle of 35° to set in motion the layer and then rapidly fixed at a lower angle until the flowing layer stops or reaches a stationary state. The inclination is fixed by adjusting the direction of the gravity force. We note that the stationary state was easily reached, thanks to periodic boundary conditions along the flow direction. In that case, the local velocity field follows approximately a Bagnold profile, in agreement with previous works [24–27].

For the heap configuration, a box of $400d$ length and $20d$ width is initially filled with grains. We measure the fluid-layer thickness $\mathcal{R}$, the heap angle $\theta_{\rm heap}$, and the velocity field, for different flow rates Q. A continuous

refill at the top compensates for the continuous loss at the wall end (Fig. 2, bottom). The simulation is running until a stationary state is reached. In addition, to obtain reliable measurements for the heap configuration, several issues were solved. First, there is a drastic influence of lateral walls [28], avoided here thanks to periodic lateral boundary conditions. Secondly, producing homogeneous flows down a heap requires very large systems. Finally, as previously shown [29], stable flows cannot be obtained for very thin layers ($\mathcal{R} \leq 5$) in the heap configuration, as intermittent/unstable flows are instead observed.

* These two authors contributed equally.
† pascal.damman@umons.ac.be

[1] Jerolmack, D.J. & Daniels, K.E. Viewing Earth's surface as a soft matter landscape. *Nature Review Physics* **1**, 716–730 (2019).
[2] Bouchaud, J.-P., Cates M.E., Ravi Prakash, J., & Edwards, S.F. A model for the dynamics of sandpile surfaces. *J. Phys. I France* 1383–1410 (1994).
[3] Pouliquen, O. & Forterre, Y. A non-local rheology for dense granular flows. *Philosophical Transactions of the Royal Society A* **367**, 5091–5107 (2009).
[4] Kamrin, K. & Koval G.. Nonlocal constitutive relation for steady granular flow. *Phys. rev. lett.* **108** 178301 (2012).
[5] Bouzid, M., Trulsson, M., Claudin, P., Clément, E. & Andreotti, B. Nonlocal rheology of granular flows across yield conditions. *Phys. Rev. Lett.* **111**, 238301 (2013).
[6] Bouzid, M., Izzet, A., Trulsson, M., Clément, E., Claudin, P. & Andreotti, B. Non-local rheology in dense granular flows. *Eur. Phys. J. E* **38**, 125 (2015).
[7] Jop, P., Forterre, Y. & Pouliquen, O.. A constitutive law for dense granular flows. *Nature* **441**, 727–730 (2006).
[8] Bouchaud, J.P., Cates, M.E., Ravi Prakash, J. & Edwards, S.F.. Hysteresis and Metastability in a Continuum Sandpile Model. *Phys. Rev. Lett.* **74**, 1982–1985 (1995).
[9] Boutreux, T., Raphaël, E. & de Gennes, P.G.. Surface flows of granular materials: A modified picture for thick avalanches. *Phys. Rev. E* **58**, 4692–4700 (1998).
[10] Quartier, L., Andreotti, B., Douady, S. & Daerr, A. Dynamics of a grain on a sandpile model. *Phys. Rev. E* **62**, 8299–8307 (2000).
[11] Andreotti, B. & Douady, S. Selection of velocity profile and flow depth in granular flows. *Phys. Rev. E* **63**, 031305 (2001).
[12] Andreotti, B. A mean-field model for the rheology and the dynamical phase transitions in the flow of granular matter. *Eur. Phys. Lett.* **79**, 34001 (2007).
[13] Pouliquen, O. Scaling laws in granular flows down rough inclined planes. *Phys. Fluids* **11**, 542–548 (1999).
[14] Silbert, L.E., Ertas, D., Grest, G.S., Halsey, T.C., Levine, D. & Plimpton, S.J. Granular flow down an inclined plane: Bagnold scaling and rheology. *Phys. Rev. E* **64**, 051302 (2001).
[15] Borzsonyi, T., Halsey, T.C. & Ecke, R.E. Avalanche dynamics on a rough inclined plane. *Phys. Rev. E* **78**, 011306 (2008).
[16] Malloggi, F., Andreotti, B. & Clément, E. Nonlocal effects in sand flows on an inclined plane. *Phys. Rev. E* **91**, 052202 (2015).
[17] Kamrin, K. & Henann, D.L. Nonlocal modeling of granular flows down inclines. *Soft Matter* **11**, 179–185 (2015).
[18] Albert, R., Albert, I., Hornbaker, D., Schiffer, P. & Barabási, A.L. Maximum angle of stability in wet and dry spherical granular media. *Phys. Rev. E* **56**, R6271–R6274 (1997).
[19] Geng, J., Howell, D., Longhi, E., Behringer, R.P., Reydellet, G., Vanel, L., Clément, E. & Luding, S Footprints in Sand: The Response of a Granular Material to Local Perturbation. *Phys. Rev. Lett.* **87**, 035506 (2001).
[20] Majmudar, T. & Behringer, R. Contact force measurements and stress-induced anisotropy in granular materials. *Nature* **435**, 1079–82 (2005).
[21] Salez, T., Salez, J., Dalnoki-Veress, K., Raphaël, E. & Forrest, J.A. Cooperative strings and glassy interfaces. *PNAS* **112**, 8227–8231 (2015).
[22] Andreotti, B., Forterre, Y. & Pouliquen, O. *Granular Media: Between Fluid and Solid*. Cambridge University Press, 2013.
[23] Kloss, C., Goniva, C., Hager, A., Amberger, S. & Pirker, S. Models, algorithms and validation for opensource DEM and CFD-DEM *Prog. Comput. Fluid Dyn.* **12**, 140-152 (2012).
[24] Rajchenbach, J. Flow in powders: From discrete avalanches to continuous regime. *Phys. Rev. Lett.* **65**, 2221–2224 (1990).
[25] Silbert, L.E., Landry, J.W. & Grest, G.S. Granular flow down a rough inclined plane: Transition between thin and thick piles. *Phys. Fluids* **15**, 1–10 (2003).
[26] GDR MiDi. On dense granular flows. *Eur. Phys. J. E* **14**, 341–365 (2004).
[27] Bharathraj, S. & Kumaran, V. Cessation of a dense granular flow down an inclined plane. *Phys. Rev. Fluids 4*, 024301 (2019).
[28] Pierre, J., Forterre, Y. & Pouliquen, O. Crucial role of sidewalls in granular surface flows: Consequences for the rheology. *J. Fluid Mech.* **541**, 167-192 (2005).
[29] Lemieux, P.A. & Durian, D.J. From avalanches to fluid flow: A continuous picture of grain dynamics down a heap. *Phys. Rev. Lett.* **85**, 4273–4276 (2000).